

Conformation of Highly-Charged Gas-Phase Lysozyme Revealed by Energetic Surface Imprinting

C. T. Reimann,^{*,†} P. A. Sullivan,[‡] J. Axelsson,[§] A. P. Quist,[⊥] S. Altmann,^{||} P. Roepstorff,[×] I. Velázquez,[£] and O. Tapia[£]

Contribution from the Division of Ion Physics, Department of Materials Science, Uppsala University, Box 534, S-751 21 Uppsala, Sweden, Vapor Technologies Inc., Boulder Tech Center, 6400 Dry Creek Parkway, Boulder, Colorado 80503, Manne Siegbahn Laboratory, Frescativägen 24, S-104 05 Stockholm, Sweden, Neuroscience Research Institute, University of California, Santa Barbara, California 93106, European Molecular Biology Laboratory, Meyerhofstr. 1, 69117 Heidelberg, Germany, Department of Molecular Biology, Odense University, Campusvej 55, DK 5230 Odense M, Denmark, and Department of Physical Chemistry, Uppsala University, Box 535, S-751 21 Uppsala, Sweden

Received January 16, 1998

Abstract: We present new results from an energetic surface imprinting method which allows us to outline the general conformation of protein ions *in vacuo*. Both disulfide-bond-intact and disulfide-bond-reduced gas-phase lysozyme ions were produced by electrospray ionization and were accelerated and impacted onto graphite surfaces. The resulting surface defects, each created by a single incident ion, were imaged with scanning force microscopy. Disulfide-intact lysozyme ions created compact, slightly elliptical hillocks on the surfaces, whereas disulfide-reduced lysozyme produced more oblong, elongated hillocks. By employing a thermal model describing the response of graphite to energy deposited by an elongated incident energetic projectile, we calculated from the hillock sizes for disulfide-reduced lysozyme ($Q = 14+$) an overall length of 32.1 ± 1.6 nm. This value is close to the length we observe for apomyoglobin ($Q = 14+$), 35.5 ± 2.4 nm, although apomyoglobin and lysozyme possess significantly different numbers of amino acid residues. Based on these results, we hypothesize that aspects of a protein's native secondary structure are preserved in the gas phase, even if the tertiary structure might be non-native. We have unfolded disulfide-intact lysozyme computationally and find a qualitatively good agreement with the experimentally obtained length of disulfide-intact ($Q = 9+$) lysozyme.

Introduction

Studies of gas-phase ionized biomolecules are motivated by the growing prevalence of matrix-assisted laser desorption ionization mass spectrometry (MALDI-MS)¹ and electrospray ionization mass spectrometry (ESI-MS),² which both produce gas-phase ions of even quite massive biomolecules³ and polymers.⁴ Recently, practical questions about the conformation of gas-phase (bio)polymers have been raised. This information is important in understanding the collisional interactions of such species with surfaces⁵ and with nonreactive gases^{6–14} and also

in understanding the chemical reactions that can occur in the gas phase.^{15–23} As a further practical concern, there is currently

* Corresponding author. FAX: +46-18-555-736; Tel: +46-18-471-3872; E-mail: curt.reimann@material.uu.se.

† Department of Materials Science, Uppsala University.

‡ Vapor Technologies Inc.

§ Manne Siegbahn Laboratory.

⊥ University of California, Santa Barbara.

|| European Molecular Biology Laboratory.

× Odense University.

£ Department of Physical Chemistry, Uppsala University.

(1) Karas, M.; Hillenkamp, F. *Anal. Chem.* **1988**, *60*, 2299–2301.

(2) Fenn, J. B.; Mann, M.; Meng, C. K.; Wong, S. F.; Whitehouse, C. M. *Science* **1989**, *246*, 64–71.

(3) Chen, R.; Cheng, X.; Mitchell, D. W.; Hofstadler, S. A.; Wu, Q.; Rockwood, A. L.; Sherman, M. G.; Smith, R. D. *Anal. Chem.* **1995**, *67*, 1159–1163.

(4) Smith, R. D.; Cheng, X.; Bruce, J. E.; Hofstadler, S. A.; Anderson, G. A. *Nature* **1994**, *369*, 137–139.

(5) Jones, J. L.; Dongré, A. R.; Somogyi, A.; Wysocki, V. H. *J. Am. Chem. Soc.* **1994**, *116*, 8368–8369.

(6) Covey, T.; Douglas, D. J. *J. Am. Soc. Mass Spectrom.* **1993**, *4*, 616–623.

(7) Cox, K. A.; Julian, R. K.; Cooks, R. G.; Kaiser, R. E. *J. Am. Soc. Mass Spectrom.* **1994**, *5*, 127–136.

(8) Collings, B. A.; Douglas, D. J. *J. Am. Chem. Soc.* **1996**, *118*, 4488–4489.

(9) von Helden, G.; Wyttenbach, T.; Bowers, M. T. *Science* **1995**, *267*, 1483–1485.

(10) Clemmer, D. E.; Hudgins, R. R.; Jarrold, M. F. *J. Am. Chem. Soc.* **1995**, *117*, 10141–10142.

(11) Shelimov, K. B.; Jarrold, M. F. *J. Am. Chem. Soc.* **1996**, *118*, 10313–10314.

(12) Shelimov, K. B.; Clemmer, D. E.; Hudgins, R. R.; Jarrold, M. F. *J. Am. Chem. Soc.* **1997**, *119*, 2240–2248.

(13) Shelimov, K. B.; Jarrold, M. F. *J. Am. Chem. Soc.* **1997**, *119*, 2987–2994.

(14) Valentine, S. J.; Anderson, J. G.; Ellington, A. D.; Clemmer, D. E. *J. Phys. Chem.* **1997**, *101*, 3891–3900.

(15) McLuckey, S. A.; van Berkel, G. J.; Glish, G. L. *J. Am. Chem. Soc.* **1990**, *112*, 5668–5670.

(16) Loo, R. R. O.; Winger, B. E.; Smith, R. D. *J. Am. Soc. Mass Spectrom.* **1994**, *5*, 1064–1071.

(17) Winger, B. E.; Light-Wahl, K. J.; Smith, R. D. *J. Am. Soc. Mass Spectrom.* **1992**, *3*, 624–630.

(18) Hunter, A. P.; Severs, J. C.; Harris, F. M.; Games, D. E. *Rap. Comm. Mass Spectrom.* **1994**, *8*, 417–422.

(19) Wood, T. D.; Chorus, R. A.; Wampler, F. M. III; Little, D. P.; O'Connor, P. B.; McLafferty, F. W. *Proc. Natl. Acad. Sci. U.S.A.* **1995**, *92*, 2451–2454.

(20) Gross, D. S.; Schnier, P. D.; Rodriguez-Cruz, S. E.; Fagerquist, C. K.; Williams, E. R. *Proc. Natl. Acad. Sci. U.S.A.* **1996**, *93*, 3143–3148.

(21) Schnier, P. D.; Gross, D. S.; Williams, E. R. *J. Am. Chem. Soc.* **1995**, *117*, 6747–6757.

(22) Cassady, C. J.; Carr, S. R. *J. Mass Spectrom.* **1996**, *31*, 247–254.

keen interest in probing specific noncovalent biomolecular complexes by MS,^{24,25} and the gas-phase conformation might greatly affect the viability of specific complexes. Finally, the gas-phase environment appears to be a unique one for proteins in that there is a complete absence of water, which is normally thought to play a key role in the folding and stability of many proteins^{26–28} as well as possibly affecting the specificity of protein–ligand binding.²⁹ Thus, the role of water can be reexamined, and other interactions affecting protein conformation can be independently studied.³⁰

Recent experiments explore the apparent “openness” of gas-phase biomolecular structures by monitoring the mass shift that occurs as accessible labile hydrogens undergo hydrogen–deuterium exchange *in vacuo*.¹⁹ Other studies of ion–molecule interactions, particularly those associated with charge stripping, provide additional clues about gas-phase conformation.^{16,17} In recent studies, apparent gas-phase basicity values were extracted from charge-stripping reaction rates.^{20,21} These values are strongly influenced by the Coulomb interactions between the charge adducts and hence are thought to reflect the overall structure of the gas-phase molecular ions.²¹ Similar information is deduced from the kinetic energy released during the dissociation of small charged complexes, combined with suitable modeling.^{31–33} Finally, collisional energy loss^{6,7} and ion mobility^{9–13} measurements provide good estimates of the cross-sectional areas of electrosprayed protein ions^{6–8,10–14} and polymer ions produced by MALDI.⁹ These techniques also identify multiple conformers¹⁰ and changes in conformation.¹¹

Despite the abundant clues provided by the techniques described above, there currently exist no methods for establishing the detailed structure of gas-phase biomolecular ions. In the hopes of providing further complementary information, we have exploited a visually oriented approach toward structural elucidation of gas-phase protein ions. Using the multiply charged macromolecular accelerator (MUMMA),^{34–43} protein

ions produced by ESI are extracted from a mass spectrometer to form an ion beam and are accelerated to impact a target at a selected total kinetic energy typically in the range 100–300 keV. As each incident ion penetrates and interacts collisionally with the surface, the energy deposited diffuses and dissipates, resulting in a surface defect which can be measured by scanning probe microscopy (SPM).^{44,45} The shape of each defect reflects the conformation and orientation of the incident ion which created it. In earlier work, we have used this method to explore the gas-phase conformations of several kinds of proteins.^{40–43} Also, we studied the structure and fragmentation of poly(ethylene glycols).⁴² In a parallel set of studies employing the MUMMA, we observed indirect effects of protein conformation via measurements of particle-impact-induced emission of secondary electrons³⁶ and secondary ions.³⁸

In this paper, we present new results comparing surface imprints created with energetic disulfide-bond-intact (DI-LYZ) and disulfide-bond-reduced lysozyme (DR-LYZ). A comparison to our previous data on apomyoglobin (AMYO)^{40,41} strengthens the hypothesis that *highly charged* proteins tend to be globally denatured in the gas phase while maintaining significant vestiges of second-order structure, viz. α -helices. An extended abstract of some of these results was already published.⁴⁶

None of the experimental techniques described above, including the method explored herein, provides detailed atomic coordinates. Molecular dynamics (MD) simulations can be used to provide such information. If the protein–solvent interactions, absent *in vacuo*, can be removed without changing the intra-protein interactions, the resulting force field can be retained to simulate the biomolecule in the absence of H₂O. This can be done with the GROMOS⁴⁷ force field. In this paper, an electroneutral protein force field was employed to explore the structural properties of DI-LYZ. Inclusion of a weak systematic centrifugal force created unfolding conditions. We present below a subset of results on unfolding of DI-LYZ as pertaining to the present experimental study.⁴⁸

Experimental and Computational Methods

Preparation of Disulfide-Intact and Disulfide-Reduced Lysozyme. Hen-egg DI-LYZ (14306.2 u, Sigma, St. Louis, Mo.) was used with no purification. DR-LYZ (15155.3 u) was obtained from DI-LYZ by reducing the disulfide bonds with DL-dithiothreitol (DTT) in 6 M guanidine hydrochloride (0.5 M Tris·HCl, pH 7.6), alkylating (“capping”) the reduced disulfide bonds with 4-vinylpyridine, and purifying the resulting solution by high-pressure liquid chromatography (HPLC).⁴⁹ Solutions were prepared for ESI by adding 4% acetic acid to a combination of equal volumes of $\approx 10^{-5}$ M protein-water solution and methanol. The pH of the solutions was 3.1. ESI mass spectra of DI-LYZ and DR-LYZ, acquired by employing the MUMMA in the conventional ESI-MS mode, are shown in Figure 1.

(23) Kaltashov, I. A.; Fenselau, C. *Proteins: Struct., Funct. Gen.* **1997**, *27*, 165–170.

(24) Przybylski, M.; Glocker, M. O. *Angew. Chem. Int. Ed. Engl.* **1996**, *35*, 806–826.

(25) Loo, J. A. *Bioconjugate Chem.* **1995**, *6*, 644–665.

(26) Lazaridis, T.; Karplus, M. *Science* **1997**, *278*, 1928–1931.

(27) Dill, K. A.; Bromberg, S.; Yue, K. Z.; Fiebig, K. M.; Yee, D. P.; Thomas, P. D.; Chan, H. S. *Protein Science* **1995**, *4*, 561–602.

(28) Dill, K. A. *Biochem.* **1990**, *29*, 7133–7155.

(29) Ladbury, J. E. *Chem. Bio.* **1996**, *3*, 973–980.

(30) Wolynes, P. G. *Proc. Natl. Acad. Sci. U.S.A.* **1995**, *92*, 2426–2427.

(31) Adams, J.; Strobel, F. H.; Reiter, A.; Sullards, M. C. *J. Am. Soc. Mass Spectrom.* **1996**, *7*, 30–41.

(32) Kaltashov, I. A.; Fenselau, C. C. *J. Am. Chem. Soc.* **1995**, *117*, 9906–9910.

(33) Szilágyi, Z.; Drahos, L.; Vékey, K. *J. Mass Spectrom.* **1997**, *32*, 689–696.

(34) Håkansson, P.; Della-Negra, S.; Mouffron, J. P.; Waast, B.; Sullivan, P. A. *Nucl. Instrum. Methods Phys. Res. B* **1996**, *112*, 39–47.

(35) Axelsson, J.; Parilis, E. S.; Reimann, C. T.; Sullivan, P.; Sundqvist, B. U. R. *Nucl. Instrum. Methods Phys. Res. B* **1995**, *101*, 343–356.

(36) Axelsson, J.; Reimann, C. T.; Sundqvist, B. U. R. *Nucl. Instrum. Methods Phys. Res. B* **1994**, *88*, 131–137.

(37) Axelsson, J.; Reimann, C. T.; Sundqvist, B. U. R. *Int. J. Mass Spectrom. Ion Proc.* **1994**, *133*, 141–155.

(38) Zubarev, R. A.; Bitensky, I. S.; Demirev, P. A.; Sundqvist, B. U. R. *Nucl. Instrum. Methods Phys. Res. B* **1994**, *88*, 143–148.

(39) Sullivan, P. A.; Axelsson, J.; Sundqvist, B. U. R. *Rapid Comm. Mass Spectrom.* **1995**, *9*, 377–382.

(40) Sullivan, P. A.; Reimann, C. T.; Axelsson, J.; Altmann, S.; Quist, A. P.; Sundqvist, B. U. R. *J. Am. Soc. Mass Spectrom.* **1996**, *7*, 329–341.

(41) Reimann, C. T.; Sullivan, P. A.; Türpitz, A.; Altmann, S.; Quist, A. P.; Bergman, A.; Oscarsson, S. O.; Sundqvist, B. U. R.; Håkansson, P. *Surf. Sci. Lett.* **1995**, *341*, L1019–L1024.

(42) Reimann, C. T.; Quist, A. P.; Kopniczyk, J.; Sundqvist, B. U. R.; Erlandsson, R.; Tengvall, P. *Nucl. Instrum. Methods Phys. Res. B* **1994**, *88*, 29–34.

(43) Quist, A. P.; Ahlborn, J.; Reimann, C. T.; Sundqvist, B. U. R. *Nucl. Instrum. Methods Phys. Res. B* **1994**, *88*, 164–169.

(44) Quate, C. F. *Surf. Sci.* **1994**, *299/300*, 980–995.

(45) Rohrer, H. *Surf. Sci.* **1994**, *299/300*, 956–964.

(46) Sullivan, P. A.; Reimann, C. T.; Axelsson, J.; Quist, A. P.; Håkansson, P.; Sundqvist, B. U. R. In *44th ASMS Conference on Mass Spectrometry and Allied Topics*; Portland, OR, 1996; pp 775–776.

(47) van Gunsteren, W. F.; Berendsen, H. J. C. *Groningen Molecular Simulation (GROMOS) Library Manual*; Biomos: Nijenborgh 16, 9747 AG Groningen, The Netherlands, 1987.

(48) Reimann, C. T.; Velázquez, I.; Tapia, O. *J. Phys. Chem. B* **1998**, *102*, 2277–2283.

(49) Thomsen, J.; Bayne, S. J. *Protein Chem.* **1988**, *7*, 295–296.

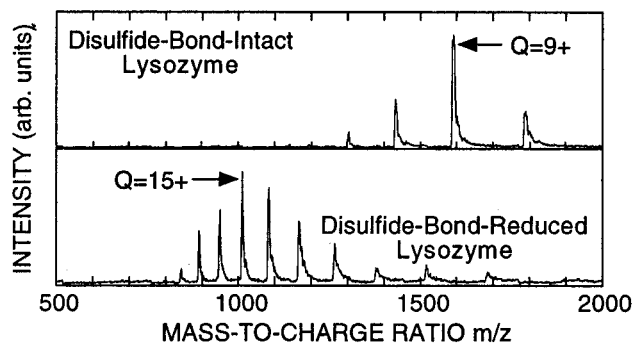


Figure 1. Electrospray ionization mass spectrometry (ESI-MS) spectra of disulfide-bond-intact (DI-, top) and disulfide-bond-reduced (DR-, bottom) hen-egg lysozyme (LYZ). Note the mass shift due to capping the exposed cysteine side chains with 4-vinylpyridine. The most probable charge state for each spectrum is shown.

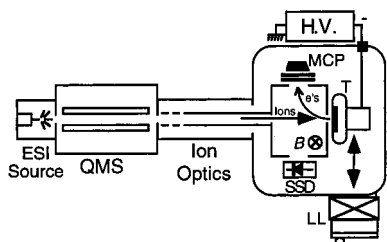


Figure 2. Schematic diagram of the multiply charged macromolecular accelerator (MUMMA).^{34,50} ESI = electrospray ionization; QMS = quadrupole mass spectrometer; H.V. = high voltage; MCP = multi-channelplate detector; SSD = solid-state detector; T = target; LL = load-lock chamber for sample introduction; and *B* is a switchable magnetic field for detecting secondary electrons (e^- s) with either the MCP (for counting of the incident ions) or the SSD (for statistical analysis of secondary electron emission).

Multiply-Charged Macromolecular Accelerator. The MUMMA³⁴ is based on a commercial ESI source⁵⁰ interfaced with a quadrupole mass spectrometer (QMS). A schematic of the experimental apparatus is shown in Figure 2. The infusion rate of protein solution into the spraying needle is 1 μ L/min, and the repeller voltage in the ESI source is typically ≈ 10 V. Ions transmitted by the QMS are fashioned into an ion beam by extraction optics. The ions are directed toward and accelerated onto a target biased at a negative potential as high as -20 kV. As each ion impacts the target, a pulse of secondary electrons is emitted and accelerated to ground potential to be detected with high efficiency in a dual-channelplate detector assembly (for pulse counting) or in a solid-state detector (for analysis of the number of secondary electrons emitted per impact).

By scanning the QMS, the MUMMA can be employed as an ESI mass spectrometer (Figure 1). Alternatively, a selected ionic species can be extracted from the QMS and used to bombard a target surface. Previous studies have shown that the number of emitted electrons is correlated with the mass of the impacting ion and that the observation of a well-defined secondary electron number distribution is indicative of a well-focused ion beam consisting of intact protein ions.^{37,51,52}

Bombardment of Targets; Microscopic Analysis. Before carrying out a bombardment, a blank target was loaded into

the system for acquiring ESI mass spectra, selecting a desired bombarding species, and optimizing the ion beam. Then, freshly cleaved pieces of highly oriented pyrolytic graphite (HOPG, Advanced Ceramics Corp., Cleveland, U.S.A.) were loaded into the system for bombardment. Targets were bombarded with either DI-LYZ or DR-LYZ in selected charge states. The impact kinetic energy was adjusted to 146 keV (e.g., 120 eV/C-atom) by using an accelerating potential of $-146/Q$ kV, where *Q* is the charge state of the protein ion selected by the QMS. Bombardments were carried out for long enough times to register $\approx 10^8$ impacts in an area of ≈ 2 mm². After irradiation, the bombarded surfaces were analyzed with ambient scanning force microscopy (SFM) on a NanoScope III (Digital Instruments, Santa Barbara, CA) using the tapping mode. The surfaces were probed with NanoProbe silicon tips with nominal radius of curvature ≈ 10 nm and cone angle $\approx 30^\circ$.

Analysis of Energetic Surface Imprints. The mechanical response of surfaces to energetic ion impacts has been extensively studied. The polyatomic protein ions studied here interact via screened nuclear collisions between protein atoms and target atoms (their speed is less than the Bohr velocity, $\approx 2.2 \times 10^6$ m·s⁻¹). By virtue of the large number of simultaneously arriving atoms, a very large energy density is deposited in the target surface by each incident polyatomic particle, resulting in the formation of a stable, nanometer-scale surface defect due to each incident particle impact. Matthew et al. were the first to observe and quantify (using an evaporative thermally activated spike model) such surface defects, generated in carbon foils and other targets by massive H₂O cluster impacts.⁵³ Numerous workers have studied surface defect formation in HOPG by incident particles, including kilo-electronvolt atomic ions,^{54,55} small atomic clusters,^{56,57} small molecular clusters,^{58,59} large atomic clusters,⁶⁰ and protein ions.^{40–43} The resulting surface defects are mostly visualized as hillocks with SPM techniques, although craters can be imaged when sufficiently sharp probe tips are used.^{56–60}

The appearance of the surface defects in our present and previous studies^{40–43} suggests that elongated conformations are typical of many highly charged gas-phase proteins. However, the direct extraction of information on the protein conformation is not straightforward: the SFM images of hillocks are broadened relative to their actual dimensions by virtue of the *finite size* of the SFM probe tip,^{40,61} the energy deposited in each impact undergoes *transport* and induces material modification processes after which the resulting surface defect is larger than the area directly impacted by the protein (Figures 3 and 5); and the protein ions impact the surface in various *orientations* (Figures 3 and 4), yielding different defect sizes for the same conformation.

(53) Matthew, M. W.; Beuhler, R. J.; Ledbetter, M.; Friedman, L. *Nucl. Instrum. Methods Phys. Res. B* **1986**, *14*, 448–460.

(54) Marton, D.; Bu, H.; Boyd, K. J.; Todorov, S. S.; Al-Bayati, A. H.; Rabalais, J. W. *Surf. Sci.* **1995**, *326*, L489–L493.

(55) Li, T.; King, B. V.; MacDonald, R. J.; Cotterill, G. F.; O'Connor, D. J.; Yang, Q. *Surf. Sci.* **1994**, *312*, 399–410.

(56) Bräuchle, G.; Richard-Schneider, S.; Illig, D.; Rockenberger, J.; Beck, R. D.; Kappes, M. M. *Appl. Phys. Lett.* **1995**, *67*, 52–54.

(57) Reimann, C. T.; Andersson, S.; Brühwiler, P.; Mårtensson, N.; Olsson, L.; Erlandsson, R.; Henkel, M.; Urbassek, H. M. *Nucl. Instrum. Methods Phys. Res. B* **1998**, *140*, 159–170.

(58) Baba, S.; Katakuse, I.; Ikeya, M. *Solid State Phys.* **1991**, *26*, 317–322.

(59) Katakuse, I.; Baba, S.; Ichihara, T.; Ikeya, M. *Japan. J. Appl. Phys. Part 1* **1992**, *31*, 1245–1247.

(60) Seki, T.; Kaneko, T.; Takeuchi, D.; Aoki, T.; Matsuo, J.; Insepov, Z.; Yamada, I. *Nucl. Instrum. Methods Phys. Res. B* **1997**, *121*, 498–502.

(61) Odin, C.; Aimé, J. P.; Kaakour, Z. E.; Bouhacina, T. *Surf. Sci.* **1994**, *317*, 321–340.

(50) Allen, M. H.; Vestel, M. L. *J. Am. Soc. Mass Spectrom.* **1992**, *3*, 18.

(51) Bondarenko, P. V.; Grant, P. G.; Macfarlane, R. D. *Int. J. Mass Spectrom. Ion Proc.* **1994**, *131*, 181.

(52) Xu, Y.; Bae, Y. K.; Beuhler, R. J.; Friedman, L. *J. Phys. Chem.* **1993**, *97*, 11883–11886.

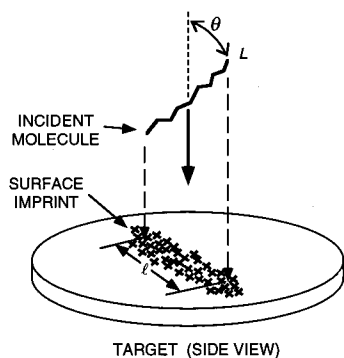


Figure 3. Schematic diagram of an extended, narrow stick-like protein ion creating a surface imprint on impact. L is the length of the protein, and θ is the polar orientation angle. The projected length of the protein on the surface is $l = L \cdot \sin(\theta)$. The actual length of the surface imprint (x 's) exceeds $L \cdot \sin(\theta)$ because of the transport of deposited energy; see Figure 5.

Finite Size of Probe-Tip. A correction was made for finite SFM probe tip size in evaluating the lateral dimensions of the surface defects. The apparent increase in lateral dimensions due to the imaging of a hillock of width w and height h by a probe tip of radius $R \approx 10$ nm is $\Delta w \approx 2Rh w^{-1}$, and observed width and length values were corrected by this amount before further processing.⁴⁰ Variations in R by $\pm 20\%$ produced variations in evaluated lateral dimensions which were much smaller than the final range of conformer lengths deduced for each species studied (discussed below; see Table 1).

Energy Transport. Energy diffusion and surface modification lead to a broadening of the surface defects; if this broadening can be subtracted, higher resolution information on the region impacted by the protein ion—and thus on the conformation of the protein ion itself—can be obtained.

A sophisticated treatment of surface defect formation by single cluster impact was given by Insepov and Yamada,⁶² but we employ here a more simple approach analogous to that of Szenes.⁶³ We argue that the surface defects are caused by a thermally activated process such as melting-resolidification to form an amorphous zone.⁶⁴ Since HOPG is highly anisotropic,⁶⁵ the two-dimensional heat diffusion equation is employed to model such processes.^{40,66}

We adapted the heat diffusion equation to a line source of energy of length l in the plane of the surface to describe an impact event. The deposited energy density⁴⁰ depends on the time (t) and spatial coordinates (ρ , ζ) as

$$\epsilon(\rho, \zeta, t) = \frac{1}{2\sqrt{\pi}} \frac{\Delta E_i}{l c} \frac{1}{\sqrt{4\kappa t}} \exp\left(-\frac{\rho^2}{4\kappa t}\right) \left[\operatorname{erf}\left(\frac{l-2\zeta}{2\sqrt{4\kappa t}}\right) + \operatorname{erf}\left(\frac{l+2\zeta}{2\sqrt{4\kappa t}}\right) \right] \quad (1)$$

where ρ and ζ are defined in Figure 5, κ is the thermal diffusivity in the basal plane of HOPG, l_c is the lattice spacing perpendicular to the basal plane, and ΔE_i is the amount of energy deposited by the incident projectile per monolayer. Using a melting energy of 2.4 eV \cdot atom⁻¹, eq 1 numerically yields a

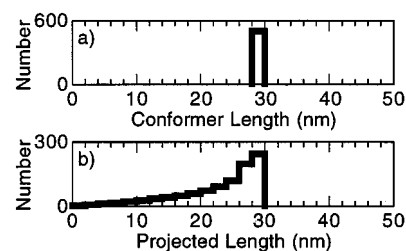


Figure 4. (a) Population histogram of 1000 particles uniformly distributed in conformer length L in the range 28–30 nm. (b) Projected length l distribution histogram for the L population distribution in (a) convoluted with the theoretical distribution $g(l)$ described in the text. The distribution is skewed and peaks at the projectile length L .

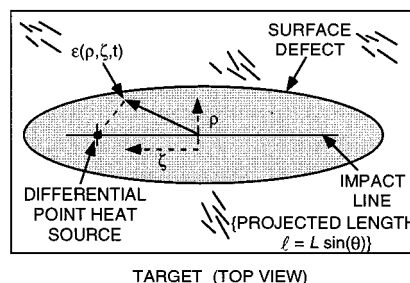


Figure 5. Energy transport from the impact line given by the projected length $l = L \cdot \sin(\theta)$ of the incident molecule creates a melted and resolidified region which is visualized by scanning force microscopy (see also Figure 3). ρ and ζ are the spatial coordinates, and $\epsilon(\rho, \zeta, t)$ is the time-dependent radial profile of the energy density given in the text. $\epsilon(\rho, \zeta, t)$ is found by solving the two-dimensional heat-diffusion equation for a set of differential point heat sources along the impact line of length l .⁴⁰

melted zone, the dimensions of which can be fitted to the dimensions of a given surface defect (after correction for probe-tip size) via the parameters l and ΔE_i . l is the projected length of the protein—the length of the region actually impacted directly by the protein—which caused the given surface defect. The value of the thermal diffusivity does not affect the values of the fitting parameters. Although the model does not explicitly consider energy lost due to ejection of material from the central portion of the defect, approximately, this would affect only the fitted value of ΔE_i , not the form of eq 1 or the fitted value of l .

Orientation. Since the kinetic energy per atom in the impacting protein greatly exceeds the atomic binding energy, it is justified to assume that the protein does not reorient due to impact. Thus, physical length L and projected length l are connected by $l = L \cdot \sin(\theta)$, where θ is the polar angle of orientation of the protein long axis (Figure 3). Random orientation as well as tumbling with randomly oriented spin axis of elongated particles of physical length L leads to a distribution of projected lengths l on the surface sharply skewed toward, and possessing one peak at, the maximum length L .⁴⁰ The projected length distribution $g(l)$ for an ensemble of such particles is $g(l) = l \cdot L^{-1} \cdot (L^2 - l^2)^{-1/2}$. A histogram of this function—convoluted with a uniform distribution of lengths L in a particular narrow range—is shown in Figure 4.

In general the overall center of charge and the center of mass do not overlap in a given conformer, causing a torque roughly parallel to the target plane to act on each ion during final acceleration. In the extreme instance of elongated conformers with initially stationary (though random) orientation, this torque enhances the contribution of relatively end-on impacts (small projected lengths) with respect to the distribution shown in Figure 4, due to induced pendular motion perpendicular to the

(62) Insepov, Z.; Yamada, I. *Mater. Sci. Eng. A* **1996**, 217–218, 89–93.

(63) Szenes, G. *Phys. Rev. B* **1995**, 51, 8026–8029.

(64) Agranat, M. B.; Ashitkov, S. I.; Kirillin, A. V.; Kostanovskii, A. V.; Fortov, V. E.; Anisimov, S. I.; Kondratenko, P. S. *JETP-Lett.* **1997**, 66, 699–703.

(65) Dresselhaus, M. S.; Kalish, R. *Ion Implantation in Diamond, Graphite and Related Materials*; Springer-Verlag: Berlin, 1992.

(66) Bräuchle, G.; Richard-Schneider, S.; Illig, D.; Beck, R. D.; Schreiber, H.; Kappes, M. M. *Nucl. Instrum. Methods Phys. B* **1996**, 112, 105–108.

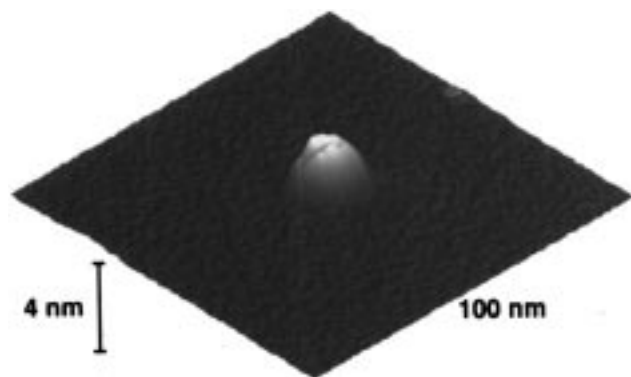


Figure 6. Zoomed surface plot of one hillock created by an incident 146-keV DI-LYZ ion (charge state $Q = 9+$). A vestige of a crater is seen running along the ridge of the hillock. The height and gray scales were chosen to highlight the existence of the crater.

target plane; however, a sharp peak at the maximum conformer length still occurs in the projected length distribution. More typically, the existence of rotation/tumbling prior to acceleration may stabilize the conformer against the action of torque, yielding a projected length distribution very similar to $g(l)$ given above.

Figure 4 shows that a broad distribution of conformer lengths is not required to explain a broad distribution of surface defect lengths. Indeed, a narrow range of conformer lengths yields a quite broad distribution of projected lengths on the surface. It is seen generally from Figure 4 that the imprinting method emphasizes side-on impacts. Therefore, to extract from a projected length (l) distribution the physical length (L) characterizing the conformers, one should focus on the longer surface defects. In the defect length histograms to be presented below, we focused on events which lay in the range between the most represented length (i.e., the peak) and that greater length for which the probability for observation was reduced by $\approx 50\%$. Then, within those length limits, we determined the range of width values which encompassed half the observed events. The result was a box on a plot of length vs width (Figures 7–9); the center of the box is characteristic of the population of conformers, while the box size yields uncertainties in extracted parameters. In each set of data, we considered also the single surface defect which had the maximum length. Using the deduced length/width pairs, correcting for the finite size of the probe tip, and using the fact that the impacts are side-on, i.e., $l = L \cdot \sin(\theta) = L$ for $\theta = 90^\circ$, we used eq 1 to extract L for characteristic and longest conformers (Method 1 in the Table).

The observed projected length histograms (after correction for energy transport and finite probe tip size) can be modeled as a sum of histograms of the type shown in Figure 4b. Our model is that the conformer length population distribution within one histogram bin—here 2 nm wide—is constant, but that the number of conformers in each bin i , a_i , can vary. The sharp cutoff of the contribution to the total projected length distribution of the conformer a_i above its maximum projected length means that the populations a_i can be calculated sequentially from the data histograms starting from the longest length present in each data set. Errors in the histogrammed data are taken to be Poissonian and propagation of errors throughout the procedure to extract the populations a_i yields the population uncertainties δa_i . A plot of a_i vs L then yields the most probable conformer length and its spread (Method 2 in the Table).

Computational Unfolding of Disulfide-Intact Lysozyme.

Our molecular dynamics (MD) studies of LYZ are described in depth elsewhere.⁴⁸ Briefly, the atomic coordinates from the X-ray structure of wild-type hen egg-white DI-LYZ at 0.17 nm

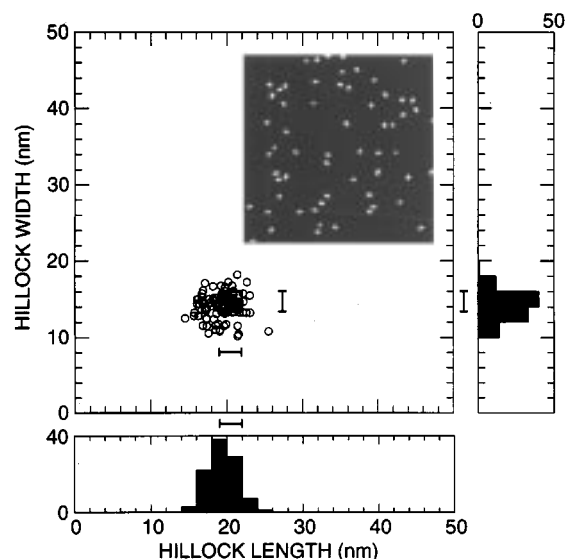


Figure 7. Image ($500 \times 500 \text{ nm}^2$) of slightly oblong surface defects created by incident energetic DI-LYZ ($Q = 9+$) and corresponding length and width histograms and plot of width versus length. 100 surface defects were measured. A box and range bars show the characteristic points taken to be representative of the longest defects (see also Figures 8 and 9). The height and gray scales were chosen to highlight the lateral extent of the surface defects.

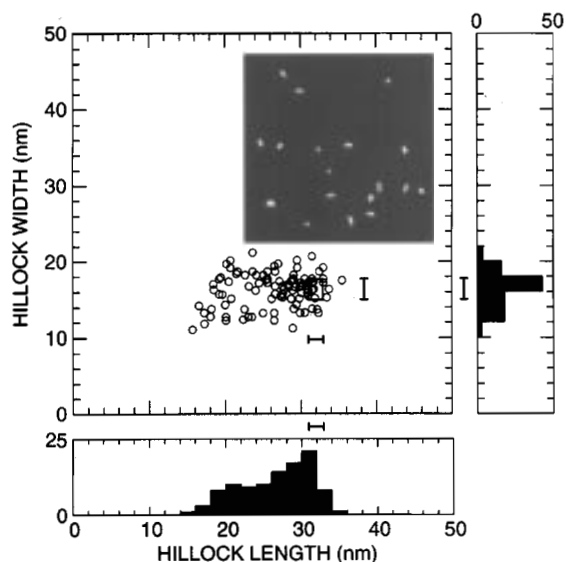


Figure 8. Image ($500 \times 500 \text{ nm}^2$) of generally elongated surface defects created by incident energetic DR-LYZ ($Q = 10+$), and corresponding length and width histograms and plot of width versus length. 102 surface defects were measured.

resolution⁶⁷ were obtained from the Brookhaven protein data bank (E.C.3.2.1.17; PDB #1hel). The coordinates of the polar hydrogens (not available from the database) were generated from standard geometries, and cycles of energy minimization were carried out to remove concomitant intramolecular stresses. MD computations, seeded with the energy-minimized coordinates, were then performed using the GROMOS-87 D4 force field⁴⁷ within the electroneutral framework.⁶⁸ That the whole set of interactions is balanced can be inferred from the protein stability around the X-ray structure observed for the 1 ns trajectory

(67) Wilson, K. P.; Malcolm, B. A.; Matthews, B. W. *J. Biol. Chem.* **1992**, *267*, 10842.

(68) Åqvist, J.; van Gunsteren, W. F.; Leijonmarck, M.; Tapia, O. *J. Mol. Biol.* **1985**, *183*, 461–477.

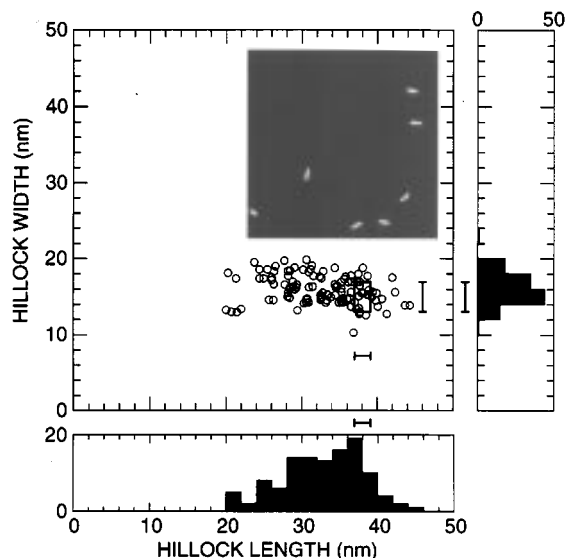


Figure 9. Image ($500 \times 500 \text{ nm}^2$) of highly elongated surface defects created by incident energetic DR-LYZ ($Q = 14+$), and corresponding length and width histograms and plot of width versus length. 114 surface defects were measured.

simulation carried out for DI-LYZ under weak coupling to a Berendsen thermal bath.⁶⁹

The point of the electroneutral framework⁶⁸ is to model the electrical shielding of protein charges by H_2O solvent and counterions without including the mass of the solvent. Thus, one effectively models the behavior of an electrically neutral protein in the gas phase. However, the Berendsen thermal bath⁶⁹ has been associated with a certain peculiarity: under the right conditions, kinetic energy can be transferred between the internal and global modes of the protein.⁷⁰ In our simulations of DI-LYZ with *strong* coupling to the Berendsen thermal bath, this effect led to spinning of the model protein, and a radial centrifugal force caused the protein to unfold. As discussed below, the effect of a radial centrifugal force is to qualitatively simulate the unfolding effect of a radial, repulsive Coulomb force, which might act to destabilize highly charged gas-phase proteins.

Results

Electrospray Ionization and Most Probable Charge States.

As shown (Figure 1), the ESI-MS charge-state envelope for DI-LYZ peaked at $Q = 9+$, while the charge-state envelope for DR-LYZ peaked at $Q = 15+$. Such changes in the charge state envelope are often observed when globular proteins stabilized by disulfide bonds have these bonds reduced; the changes are thought to reflect conformational changes in the solution phase.

Surface Defects Formed by Energetic Lysozyme Ions.

Surface defects induced by DI-LYZ⁹⁺ appeared as compact, slightly oval hillocks. The observed protrusions were robust under repeated imaging and thus represent localized surface defects, not sputtered/displaced loose debris. A zoomed view of one such hillock reveals vestiges of a crater along the ridge (Figure 6). The hillocks were characterized by an aspect ratio (length-to-width ratio) of ≈ 1.4 (Figure 7). Compared to our previous measurements,⁴⁰ we employed a finer probe tip in the present measurements, since the ovalarity was more easily observed, since both lengths and widths appeared typically

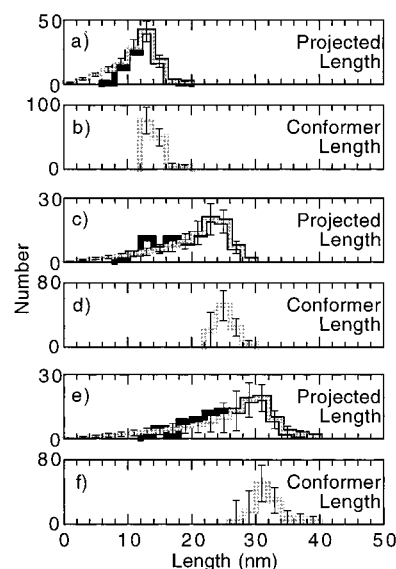


Figure 10. (a) Black line: Projected length l histogram for DI-LYZ, $Q = 9+$, after correction for finite-size probe tip and energy transport as discussed in the text. Grey line: Projected length histogram for the population of conformer lengths L given in (b). (c) and (d) Same as (a) and (b) but for DR-LYZ, $Q = 10+$. (e) and (f) Same as (a) and (b) but for DR-LYZ, $Q = 14+$.

smaller than previously reported,⁴⁰ and since we resolved vestiges of impact craters, also not observed previously by us for HOPG targets.⁴⁰

Widths we observed were similar to widths observed (3–18 nm) in high-resolution scanning tunneling microscopy images of surface defects created by compact incident polyatomic projectiles such as C_{60} , Ar_{100} , and $(\text{CsI})_n$.^{56,59,60} An exact quantitative correspondence in this regard was not expected because the impact geometry is very different for elongated proteins (discussed below) and since different kinetic energies were used.

Surface defects induced by DR-LYZ¹⁰⁺ (Figure 8) were often noticeably elongated with respect to the hillocks shown in Figure 7, displaying aspect ratios ranging up to ≈ 1.8 based on the peaks of the length and width distributions. Surface defects induced by DR-LYZ¹⁴⁺ were even more elongated than the ones induced by DR-LYZ¹⁰⁺ with aspect ratios ranging up to ≈ 2.5 (Figure 9).

For both characteristic conformers (see boxes on the length vs width plots in Figures 7–9) and the individual longest defects defined above, the thermal model of eq 1 was applied to find the best value for conformer length. The results are shown in Table 1 (Method 1), where information⁴⁰ for AMYO¹⁴⁺ is also included.

A histogram of the projected length distribution for a set of conformers narrowly distributed in length (see viz. Figure 4) is somewhat narrower at its peak than observed projected length distributions (Figures 8 and 9). Moreover, the observed distributions do not abruptly terminate but rather display tails at higher lengths. This observation can reflect the existence of an ensemble of proteins characterized by a *range* of lengths.

For DI-LYZ⁹⁺ the upper four projected length l histogram bins (after correction for probe-tip size and energy diffusion; Figure 10a) were fitted to yield an asymmetric distribution of conformer population in physical lengths $L = 12$ –20 nm (Figure 10b). The most probable length was 13 nm; the full-width at half-maximum (fwhm) was ≈ 4 nm.

For DR-LYZ¹⁰⁺ the upper four projected length histogram bins (Figure 10c) were fitted to yield a bell-like distribution of

(69) Berendsen, H. J. C.; Postma, J. P. M.; van Gunsteren, W. F.; Nola, A. D.; Haak, J. R. *J. Chem. Phys.* **1984**, *81*, 3684–3690.

(70) Lemak, A. S.; Balabaev, N. K. *Mol. Sim.* **1994**, *13*, 177–187.

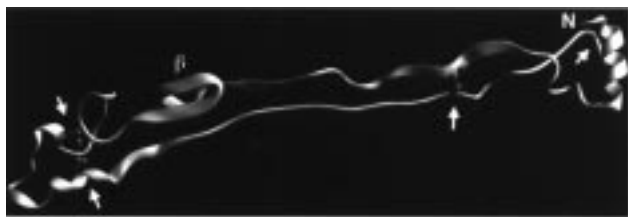


Figure 11. The structure of DI-LYZ visualized (Ribbons program, M. Carson, University of Alabama at Birmingham, CMC) after 1 ns of molecular dynamics simulation with strong coupling to a thermal bath starting from a compact, natively like structure equivalent to the X-ray crystallography structure.⁴⁸ All portions of polypeptide chain which had adopted helical or sheetlike structures in the protein database entry are depicted as wide ribbons, while the rest of the polypeptide chain is depicted as narrow strands. Disulfide bonds are shown as balls and sticks and are marked by arrows; N indicates the N-terminus; and β shows the vestiges of the β -sheet (though after 1 ns the original hydrogen bonding pattern of the β -sheet had been destroyed).

population in physical lengths 22–30 nm (Figure 10d). The most probable length was 25 nm; the fwhm was ≈ 4 nm. For DR-LYZ¹⁴⁺ the upper seven projected length histogram bins (Figure 10e) were fitted to yield a bell-like distribution of population in seven physical length bins in the range 26–40 nm (Figure 10f). The most probable length was 31 nm; the fwhm was ≈ 4 nm.

The most probable lengths derived by this method are also shown in Table 1 (Method 2) and agree substantially with the characteristic lengths. Indeed, the gross nature of the projected length distributions are fitted using a fairly narrow distribution of conformer lengths. However, in Figure 10a,b (DI-LYZ⁹⁺), the fitted distribution overestimates the data for projected lengths under 8 nm. Also, in Figure 10c,d (DR-LYZ¹⁰⁺) and Figure 10e,f (DR-LYZ¹⁴⁺) the fitting procedure underestimated the data for projected lengths in the range 12–18 and 18–26 nm, respectively, while overestimating the data for smaller projected lengths. The discrepancies probably reflect simplified aspects of the model. For example, conformers may be bent slightly (Figures 8 and 9) instead of being straight, making very small projected lengths impossible. Also, the role of torque-induced pendular motions is not considered in detail, although there is no indication of any contribution at low projected lengths that would be caused by the torque.

Computer-Simulated Unfolding of Native Lysozyme. Using weak, systematic perturbing centrifugal forces (≈ 20 eV rotational kinetic energy), we computationally drove an unfolding process of native DI-LYZ.⁴⁸ After approximately 1 ns of integrating the system, the formerly globular protein had passed through a number of conformations, ending as a conformer which was elongated to a length of ≈ 11 nm and a width of ≈ 1.1 nm (Figure 11). The spatial arrangement of disulfide bridges appeared to prevent further elongation.

Discussion

Relation of Observed LYZ Conformations to Native and Completely Extended Conformations. The shapes of the defects caused by impacts of DR-LYZ (Figures 8 and 9) suggest that gas-phase protein ions can be quite extended in their conformations. Yet they are not completely extended. DR-LYZ, with 129 amino acid residues, would stretch 46.4 nm if completely extended, and AMYO, with 153 amino acid residues, would stretch 55.1 nm if completely extended. These lengths exceed the observed ones considerably, even if no correction is made for SPM probe tip size or energy transport. Therefore,

under our experimental conditions, it can be concluded that the DR-LYZ ions did not adopt the form of completely extended polypeptide chain. It is likewise indisputable, just on the basis of the raw data (Figures 7–9), that DR-LYZ¹⁴⁺ was more extended than DR-LYZ¹⁰⁺, and that DR-LYZ¹⁰⁺ was more extended than DI-LYZ⁹⁺. The presence of disulfide bridges is likely to play a dominant role in hindering the unfolding of DI-LYZ⁹⁺.

Native lysozyme adopts a slightly oblong form of rough dimensions⁶⁷ $3 \times 3 \times 4.5$ nm³. We estimated a length of 13.5 nm for the DI-LYZ⁹⁺ conformer. This estimation, based on an extensive analysis concerning microscope imaging artifacts, conformer orientation, and energy deposition/transport, may be subject to error. However, it is sufficiently large with respect to the length of the native conformer to conclude definitively that DI-LYZ⁹⁺, observed in our experiment, is not as compact as the native conformation.

To make more detailed structural deductions from our experimental results may be considered risky. However, recent experimental and theoretical results concerning a peptide clearly suggest that α -helices are stable *in vacuo*, even when highly charged.²³ This strongly motivates an interpretation of our results on AMYO and DR-LYZ in terms of stretched but partly helical structures.

If gas-phase AMYO is assumed to maintain a helicity of $\approx 60\%$ while otherwise being stretched out as much as possible, then its predicted length would be 35.8 nm, close to the length we observed for $Q = 14+$. The protein database entry for LYZ indicates that 58 out of 129 amino acid residues participate in helix formation. If this helicity of $\approx 45\%$ is maintained for gas-phase DR-LYZ while the protein is otherwise stretched out as much as possible, the predicted length is 34.2 nm, within ≈ 2 nm of the length we observed for $Q = 14+$. (Note, in solution-phase folding of LYZ, helices form *before* the β -sheet.⁷¹ If protein folding/unfolding share common features between the solution and gas phases, then upon stretching out *in vacuo*, the β -sheet might be destroyed while leaving the helices intact.) It was these considerations which had prompted us to hypothesize that, for proteins *in vacuo* in high charge states, some aspects of secondary structure—namely extended, helical forms—are largely preserved, even though tertiary structure is destroyed.⁴⁰

Comparisons Between Conformations Deduced from Surface Imprinting and Proton-Transfer Rates. Gross et al. have studied conformations and folding of lysozyme ions in the gas phase by monitoring proton-transfer rates to various gaseous bases and measuring apparent gas-phase basicities.²⁰ From those measurements, DI-LYZ^{9+,10+} comprise an “island of stability” in that conformers occur which are as compact as the native one, whereas for higher and lower charge states, no such compact conformers occur. DI-LYZ^{9+,10+} also display conformers which are somewhat unfolded, and, particularly for DI-LYZ⁹⁺, such an unfolded conformer is dominant (70% population).²⁰ Our observations for DI-LYZ⁹⁺ are in the main suggestive of such an unfolded structure. Some of the hillocks we observed were nearly circular (length \approx width, Figure 7), consistent with impacts of compact, natively like conformers, but the resolution of the imprinting method does not permit putative compact conformers to be identified as a distinct population.

For DR-LYZ¹⁰⁺, the proton-transfer studies of Gross et al. are interpreted in terms of *one* conformer which appears to be more unfolded than DI-LYZ^{9+,10+} species but is not completely stretched out.²⁰ Our data corroborate such a structure as we

(71) Radford, S. E.; Dobson, C. M.; Evans, P. A. *Nature* **1992**, 358, 302–307.

Table 1. Conformer Lengths Derived for Some of the Gas-Phase Protein Ion Species Studied by the Energetic Surface Imprint Method^a

species	method 1		method 2	
	characteristic length (nm)	maximum length (nm)	most probable length (nm)	full-width at half-maximum of length distribution (nm)
DI-LYZ ⁹⁺	13.5 ± 3.0	20.5	13	≈4
DR-LYZ ¹⁰⁺	26.0 ± 1.7	29.1	25	≈4
DR-LYZ ¹⁴⁺	32.1 ± 1.6	38.6	31	≈4
AMYO ¹⁴⁺ (ref 40)	35.5 ± 2.4	38.5		

^a The superscript is the charge state of the ion. The lengths and methods are defined in the text.

observed a species characterized by length 26 nm (Table 1), intermediate in size between compact, natively like structures, and a completely extended structure.

Finally, proton-transfer reaction studies on DR-LYZ¹⁴⁺ were interpreted in terms of *one* conformer consisting of completely extended polypeptide chain.²⁰ Our estimated length of only 32.1 nm is not quantitatively consistent with that conclusion. There are two points to consider, however. The first is that conditions in the ESI source or along the path to the analysis portion of the experiment, possibly differing between different experimental setups, could have affected the conformation of the proteins. Indeed, collisionally activated *folding* of gas-phase proteins has recently been observed.¹³ And second, the interpretations of proton transfer studies rely on modeling the energetic contribution of Coulomb repulsion to gas-phase basicity—including structural and electrostatic shielding considerations. Different combinations of structure and dielectric constant can be selected so as to yield the same Coulomb contribution,²¹ and it can be difficult to distinguish between a completely stretched configuration and a configuration consisting of a single α -helix.

In any case, both surface imprints and proton-transfer reaction studies yield the conclusion that DR-LYZ¹⁴⁺ is more extended than DR-LYZ¹⁰⁺.

Comparisons between Conformations Deduced from Surface Imprinting and Ion Mobility Measurements. Valentine et al. have recently addressed the structure of gas-phase LYZ by ion mobility mass spectrometry experiments.¹⁴ For DI-LYZ⁹⁺ gently injected into a buffer gas at low energy, they observe a conformer which is compact although somewhat more open than the native structure of LYZ ($\approx 20\%$ greater collision cross section). For DI-LYZ⁹⁺ more violently injected into the buffer gas, they observe a conformer which is even more extended ($\approx 67\%$ greater collision cross section) and a small contribution from the more compact conformer. These results agree qualitatively with our observation of a conformer which is also to some degree elongated (Figures 6 and 7). On the basis of our MD results discussed below, and on the length we deduced for the DI-LYZ⁹⁺ conformer, 13.5 nm (Table 1), we believe we observed a significantly unfolded species which may correspond to the one observed by Valentine et al. under violent injection conditions. As pointed out above, the resolution of the surface imprinting method does not allow us to sense a distinct population of compact conformers, even if they might be present.

For DR-LYZ species taken directly from the ESI source, extended conformers with collision cross section approaching *but not equaling* that of a completely elongated polypeptide chain are observed by Valentine *et al.*, the degree of unfolding

increasing with increasing charge state.¹⁴ This agrees qualitatively with our observations (Figures 8 and 9). In the ion mobility experiments for DR-LYZ^{Q+} with $Q \geq 10+$, dominantly *one* conformer is observed for each charge state, with a very tiny contribution from a slightly more compact conformer. Surface imprint data do not show dramatic evidence for conformers more compact than the main one deduced (Figure 10c–f), in general agreement with the ion mobility results.

The ratio of collision cross sections^{13,14} for AMYO¹⁴⁺ and DR-LYZ¹⁴⁺ is 1.17, and the ratio of conformer lengths deduced from surface imprints for the same species is 1.15 ± 0.17 . The ratios are equivalent within the errors. In a relative sense, ion mobility and surface imprint data are thus seen to be in good agreement. However, Shelimov and Jarrold¹³ have shown that if an elongated AMYO conformer were as a whole to be wound slightly more compactly than an α -helix, it would display the same collision cross section as AMYO¹⁴⁺ displays experimentally. This would imply a conformer length less than ≈ 23 nm, in disagreement with our result of 35.5 nm.⁴⁰ Likewise, for DR-LYZ¹⁴⁺, Valentine et al. measured¹⁴ a collision cross section of 26.9 nm², or 0.21 nm² per amino acid residue, comparable to the value predicted if the whole LYZ protein were to occupy the conformation of an α -helix. The predicted length would then be only ≈ 19 nm, whereas we observed 32.1 nm. The discrepancy may be caused by different conditions in the respective experiments. It motivates future work designed to ferret out the detailed nature of the intramolecular interactions and structural motifs remaining after a significant degree of unfolding has taken place.

Gas-Phase Macromolecular Structure Hypothesized from Molecular Dynamics Simulations. One of the challenges of studying proteins and other macromolecules in the gas phase is to shed light on their unfolding–refolding pathways and their stability, despite the almost complete lack of specific information for seeding or constraining any theory. MD simulations will prove useful in this regard. For example, MD has been used to show that neutral⁷² and charged²³ α -helices and another type of helix⁷³ are stable *in vacuo*. Also, molecular mechanics (MM) and MD techniques have been used to show that local nonhelical structural forms can occur, viz. as adduct charges are “self-solvated” by nearby polymer⁹ or polypeptide chain.

It has been proposed that for protein ions in sufficiently high charge states, the radial forces associated with Coulomb repulsion favor the occurrence of an unfolding process.¹² DI-LYZ is a useful choice of a model protein because it may unfold in a particularly simple way. The native state is highly compact, but it consists of two main domains and a “hinge” which together are used to form an active site, having the appearance of jaws. The hinge-bending mode of LYZ has been studied with MM:⁷⁴ opening the active site by $\approx 10^\circ$ via the hinge increases the conformational energy by ≈ 12 kJ·mol⁻¹. The Coulomb potential energy would be lowered by ≈ 1000 kJ·mol⁻¹ due to unfolding a highly charged globular protein,¹² which seems to be a significant effect in comparison. However, unfolding might be restricted by the stabilization of secondary structure by hydrogen bonding and by the stabilization of other local structural formations by self-solvation of charge groups.¹² Therefore, the final form of the unfolded conformations is an open question which can be addressed by MD techniques.

(72) Daggett, V.; Levitt, M. *J. Mol. Biol.* **1992**, *223*, 1121–1138.

(73) Monoi, H. *Biophys. J.* **1995**, *69*, 1130–1141.

(74) McCammon, J. A.; Gelin, B. R.; Karplus, M.; Wolynes, P. G. *Nature* **1976**, *262*, 325–326.

LYZ has been denatured computationally, by MD, using different kinds of forces.⁷⁵ We used strong coupling of DI-LYZ to a thermal bath, which resulted in the transfer of energy from the internal modes of the protein to the global modes,⁷⁰ in this case inducing a spinning ($\approx 2000 \text{ kJ}\cdot\text{mol}^{-1}$ rotational kinetic energy) and a weak, systematic centrifugal-force-driven *radial* perturbation that drove an unfolding process analogous to Coulomb repulsion. The ending conformer was elongated to a length of $\approx 11 \text{ nm}$ and a width of $\approx 1.1 \text{ nm}$ (Figure 11). This length should be compared with our estimated length of DI-LYZ⁹⁺, $13.5 \pm 3 \text{ nm}$. We judge the agreement to be qualitatively adequate (the method used to extract the experimental length would have the greatest error for relatively compact impacting species, i.e., DI-LYZ in low charge states; unfortunately the origin of the *longest* surface defect induced by DI-LYZ⁹⁺ is unexplained). The simulated structure is far from being compact and natively like. It may correspond to a conformer of DI-LYZ observed by Valentine et al. to be unfolded by collisional activation.¹⁴

Conclusions

The study of highly charged protein ions *in vacuo* permits a unique examination of some of the factors that may affect protein folding and stability. New techniques are being developed to access the structure and dynamical behavior of such proteins as seen from a different perspective. Ion mobility measurements provide high resolution of multiple conformers and estimates of cross-sectional areas. Studies of gas-phase reaction kinetics allow partial resolution of various conformers; gross structure is available indirectly via the influence structure has on Coulomb energetics. Energetic surface imprinting is by contrast a low-resolution method which is also not geared toward monitoring dynamical changes in real time. However, it is

unique in providing the approximate length of the gas-phase species, in contrast to cross sectional areas derived by other methods. The surface imprint method is also unique in providing a "snapshot" of the ion conformation, with a time resolution as short as $\approx 0.1 \text{ ps}$ for side-on impacts.

Currently we hypothesize that conformers of disulfide-intact and disulfide-reduced lysozyme are elongated, narrow, and fairly straight, and that their lengths are narrowly distributed. Increasing the spatial resolution of the microscopy approach and applying image analysis in order to substantially enhance the data collection statistics could make it possible to resolve slight lateral collective oscillations as well as mass concentrations (the latter in case of probing incompletely unfolded conformers).

None of the available techniques for probing gas-phase protein structure yields interatomic distances which can be used as constraints for molecular dynamics simulations, though such information is available for peptides.³³ However, because of the complexities of these problems, computer-assisted techniques such as molecular dynamics are still necessary to supplement the experimental data. Our preliminary molecular dynamics study of the unfolding of native lysozyme by weak, systematic centrifugal forces revealed a conformer having a length qualitatively consistent with the length we deduced experimentally for electrospayed disulfide-bond-intact lysozyme.

Acknowledgment. The authors thank the Swedish Research Council for Engineering Sciences (TFR), the Swedish National Board for Industrial and Technical Development (NUTEK), the Swedish Natural Sciences Council (NFR), and the Knut and Alice Wallenberg Foundation. The authors also thank collaborators in the Protein Research Group, Odense, Denmark, for help in preparing disulfide-reduced lysozyme, as well as the anonymous referees who provided a generous number of helpful suggestions. Finally, members of the Ion Physics Group, Uppsala, are thanked for helpful discussions and support.

(75) Hünenberger, P. H.; Mark, A. E.; van Gunsteren, W. F. *Proteins: Struct., Funct. Gen.* **1995**, *21*, 196–213.